RESEARCH ARTICLE

A DFTB study on Au_{36}, Au_{37}, Au_{39} and Au_{40} (C_1) metallic gold nanoclusters ($AuNC_S$), the double and the triple-state degrees of degeneracy

K. Vishwanathan

K Vishwanathan. A DFTB study on Au_{36}, Au_{37}, Au_{39} and Au_{40} (C_1) metallic gold nanoclusters ($AuNC_S$), the double and the triple-state degrees of degeneracy. J Nanosci Nanomed 2023; 7(1): 01-05.

ABSTRACT

In this article, an interesting phenomenon has described the geometries and vibrational frequency of the stable AuN clusters with N=36, 37, 39 and 40. We have found all 4 clusters are having the very same C_1 point symmetry group. For the re-optimization process, the finite-differentiation method has been implemented within the Density Functional Tight Binding (DFTB) approach. The effects of the range of interatomic forces were calculated and the desired set of system Eigen frequencies (3N-6) are obtained by diagonalization of the symmetric positive semidefinite Hessian matrix. More than anything else, we have observed the vibrational spectra, which occur between 0.98 cm^{-1} and 304.48 cm^{-1} at ΔE =0. Most significantly, all the clusters had come across the double and the triple state degeneracies, which are due to the stretching and the bending mode of the vibrations through the atoms. Nevertheless, the vibrational spectrum is strongly dependent upon size, shape, and structure.

Key Words: *Gold atomic clusters; Density-functional tight-binding; Finite-difference method; Force constants; Vibrational spectrum*

INTRODUCTION

Nanoclusters have potential uses in chemical reactors, telecommunications, microelectronics, optical data storage, catalysts magnetic storage, spintronic devices, electroluminescent displays, sensors, biological markers, switches, nano-electronics, nano-optics, transducers and many other fields [1,2]. Noble metal like Rhodium (Rh), Palladium (Pd), silver (Ag), Platinum (Pt), and Gold (Au) is one kind of modish and desired material, according to their inherent resistance to oxidation and corrosion even in the moist environment [3-5]. Its physical and chemical properties appear to be entirely change as the size of metal continuously decreases into nanoscale because of the quantum size effect, surface effect, small size effect, and Macroscopic Quantum Tunnelling (MQT) effect [6-8].

In general, Noble metal (Cu, Ag, and Au) clusters have attracted much attention in scientific and technological fields because of their thermodynamic, electronic, optical and catalytic properties in nano-materials [9-11]. Especially, gold is a soft metal and is usually alloyed to give it more strength as well as a good conductor of heat and electricity, and is unaffected by air and most reagents, those are the main reasons to choose among the other metal clusters.

In this study, mainly we focus on the vibrational properties of gold atomic clusters with sizes Au_{36}, Au_{37}, Au_{39} and Au_{40} atoms, because, the vibrational properties play a major role in structural stability [12-18]. For further assistance for the readers, specifically for the general information about global minima gold structures which have been calculated by the work of Dong and Springborg can be found in those articles [19, 20]. In very short, the structures were found through a so called Genetic Algorithm (GA) in combination with Density Functional Tight Binding (DFTB) energy calculations and the steepest descent algorithm permitting a local total energy minimization. Nevertheless, in our case, we use the numerical finite-difference method along with the Density Functional Tight Binding (DFTB) approach and finally extract the vibrational spectrum from the optimized structures [21]. Overall, for a better understanding and to visualize, the detailed information is discussed in the results and discussion section.

MATERIALS AND METHODS

Theoretical and computational procedures

At first step, the DFTB is based on the density functional theory of Hohenberg and Kohn in the formulation of Kohn and Sham [22-24]. In addition, the Kohn-Sham orbitals $\psi_i(r)$ of the system of interest are expanded in terms of atom-centered basis functions $\{\varphi m(r)\}$,

$$\psi_i(r) = \sum_m c_{im}\phi_m \quad \text{m=j} \tag{1}$$

While so far the variational parameters have been the real-space grid representations of the pseudo wave functions, it will now be the set of coefficients c_{im}. Index m describes the atom, where ϕ_m is centered and it is angular as well as radially dependent. The ϕ_m is determined by self-consistent DFT calculations on isolated atoms using large Slater-type basis sets.

In calculating the orbital energies, we need the Hamilton matrix elements and the overlap matrix elements. The above formula gives the secular equations

$$\sum_m c_{im}\left(H_{mn}-\epsilon_i S_{mn}\right) = 0 \tag{2}$$

Here, c_{im}'s are expansion coefficients, ϵ_i is for the single-particle energies (or where ϵ_i are the Kohn-Sham eigenvalues of the neutral), and the matrix elements of Hamiltonian H_{mn} and the overlap matrix elements S_{mn} are defined as

$$H_{mn}=\phi_m|\hat{H}|\phi_n,\ S_{mn}=\phi_m|\phi_n \tag{3}$$

They depend on the atomic positions and on a well-guessed density $\rho(r)$. By solving the Kohn-Sham equations in an effective one particle potential, the Hamiltonian $\hat{H}$

is defined as

$$\hat{H}\psi_i(\mathrm{r}) = \epsilon_i\,\psi_i(\mathrm{r}), \hat{H} = \hat{T} + V_{eff}(\mathrm{r}) \tag{4}$$

To calculate the Hamiltonian matrix, the effective potential V_{eff} has to be approximated. Here, (ω_i) being the kinetic-energy operator $\Sigma(\hat{T}=-\frac{1}{2}\nabla^2)$ and $V_{eff}(r)$ being the effective Kohn-Sham potential, which is approximated as a simple superposition of the potentials of the neutral atoms,

$$V_{eff}(r)=\sum_j V_j^0(|r-R_j|) \tag{5}$$

V_j^0 is the Kohn-Sham potential of a neutral atom, $r_j = r - R_j$ is an atomic

Faculty of Natural Sciences and Technology, University of Saarland, 66123, Saarbrücken, Germany

Correspondence: K. Vishwanathan, Faculty of Natural Sciences and Technology, University of Saarland, 66123, Saarbrucken, Germany, E-mail: vishwak9@yahoo.com
Received: 16-Dec-2022, Manuscript No. Puljnn-22-5915; Editor assigned: 21-Dec-2022, Pre-QC No. Puljnn-22-5915 (PQ); Reviewed: 17-Jan-2023, QC No. Puljnn22-5915 (Q); Revised: 21-Feb-2023, Manuscript No. Puljnn-22-5915 (R); Published: 30-March-2023, DOI: 10.37532/puljnn.2023.7(1).1-5.

position, and R_j being the coordinates of the j^{th} atom. Finally, the short-range interactions can be approximated by simple pair potentials, and the total energy of the compound of interest relative to that of the isolated atoms is then written as,

$$E_{tot} \sum_i \in_i - \sum_j \sum_{mj}^{occ} \in_{jm_j} + \frac{1}{2} \sum_{j \neq j'} U \sum_{jj'} (|R_j - R_{j'}|),$$

$$\in_B \equiv \sum_i^{occ} \in_i - S \sum_j \sum_{mj}^{occ} \in_{j m_j} \quad (6)$$

Here, the majority of the binding energy ($\in_i$) is contained in the difference between the single-particle energies $\in_i$ of the system of interest and the single-particle energies of the isolated atoms (atom index j, orbital index m_j), $U_{jj'}(|\boldsymbol{R_j} - \boldsymbol{R_{j'}}|)$ is determined as the difference between $\in_B$ and for diatomic molecules (with E^{SCF} being the total energy from parameter free density functional calculations). In the present study, only the 5_d and 6_s electrons of the gold atoms are explicitly included, whereas the rest are treated within a frozen-core approximation [22, 24, 25].

Structural re-optimization process

In our case, we have calculated the numerical first-order derivatives of the forces ($F_{i\alpha}$, $F_{j\beta}$) instead of the numerical-second-order derivatives of the total energy (E_{tot}). In principle, there is no difference, but numerically the approach of using the forces is more accurate [21].

$$\frac{1}{M} \frac{\partial^2 E_{tot}}{\partial \boldsymbol{R}_{i\alpha} \partial \boldsymbol{R}_{j\beta}} = \frac{1}{M} \frac{1}{2ds} \left[\frac{\partial}{\partial \boldsymbol{R}_{i\alpha}} (-\boldsymbol{F}_{j\beta}) + \frac{\partial}{\partial \boldsymbol{R}_{j\beta}} (-\boldsymbol{F}_{i\alpha}) \right] \quad (7)$$

Here, F is a restoring forces which is acting upon the atoms, ds is a differentiation step-size and M represents the atomic mass, for homonuclear case. The complete list of these force constants (FCs) is called the Hessian H, which is a (3N×3N) matrix. Here, i is the component of (x, y or z) of the force on the j^{th} atom, so we get 3N [26].

RESULTS AND DISCUSSION

The optimized structure of the clusters Au_{36}, Au_{37}, Au_{39} and Au_{40}

We present the vibrational spectrum analysis of the re-optimized Au_{36}, Au_{37}, Au_{39} and Au_{40} clusters, interestingly, all of them are having the very same point group symmetry C_1 at ground state, ΔE= 0. Initially, the structures were found through a so-called Genetic Algorithm (GA) in combination with Density Functional Tight-Binding (DFTB) energy calculations and the steepest descent algorithm permitting a local total energy minimization [19]. To sum up, we have accurately predicted the vibrational frequency of the clusters, and they are very strongly dependent on the size, structure, and shape of the clusters, mainly influenced by the stretching and the bending mode vibrations of the atoms that are due to changes on the bond length fluctuations for a small step-size ds= ± 0.01 a.u. on the equilibrium coordinates [27]. By the way, for the perspective view of the structures, we have plotted with two different styles (Space-filling, Polyhedral).

The vibrational frequency (ω_i) range of the cluster Au_{36} at ΔE = 0

Table 1 shows the low (at the least) and the high (at the most) frequency range of the cluster Au_{36}, which occurs between 4.38 cm^{-1} and 302.78 cm^{-1}, and the lowest energy geometrical structural view can be seen in Figure 1. Firstly, the cluster has some low frequencies (ω_{min}) in between 4.38 cm^{-1} to 8.34 cm^{-1}, which is only for the very first 4 NVM that comes even below the scale of Far Infrared (FIR), IR-C 200 cm^{-1} to 10 cm^{-1}. Secondly, for the 5 NVM to 84 NVM, the frequency ranges occurred between 10.02-198.10 cm^{-1}, which comes within the range of Far Infrared FIR, IR-C 200cm^{-1} to 10 cm^{-1}. Thirdly, the rest of the 85 NVM to 102 NVM, is having the maximum high frequencies, which are ((ω_i) 200.71 cm^{-1} to 302.78 cm^{-1}) falling within the range of Mid Infrared MIR, IR-C 3330 cm^{-1} to 200 cm^{-1}.

The double state degeneracy (ω_i)

[{10.02, 10.38}; {17.16, 17.85}; {25.00, 25.64}; {47.10, 47.67}; {177.04, 177.85} and {221.29, 221.84}] in cm^{-1}

The triple state degeneracy (ω_i)

We do not find anything; it is clearly revealed through our spectrum calculations that have not occurred.

The vibrational frequency (ω_i) range of the cluster Au_{37} at ΔE=0

Table 2 shows the low (at the least) and the high (at the most) frequency range of the cluster Au_{37}, which occurs between 4.70 cm^{-1} and 300.67 cm^{-1}, and the lowest energy geometrical structural view can be seen in Figure 2. Firstly, the cluster has some low frequencies (ω_{min}) between 4.70 cm^{-1} to 9.59 cm^{-1}, which is only for the very first 6 NVM that comes even below the scale of Far Infrared FIR, IR-C 200 cm^{-1} to 10 cm^{-1}. Secondly, for the 7 NVM to 87 NVM, the frequency ranges occurred between 10.44 cm^{-1} to 197.79 cm^{-1}, which comes within the range of Far Infrared FIR, IR-C 200 cm^{-1} to 10 cm^{-1}. Thirdly, the rest of the 88 NVM to 105 NVM, is having the maximum high frequencies, which are ((ω_i) 201.54 cm^{-1} to 300.67 cm^{-1}) falling within the range of Mid Infrared MIR, IR-C 3330 cm^{-1} to 200 cm^{-1}.

The double and the triple state degeneracy (ω_i)

[{6.12, 6.48}; {10.44, 10.62}; {17.18, 17.87}; {29.07, 29.95}; {43.18, 43.59} and {95.22, 95.98}] in cm^{-1}.

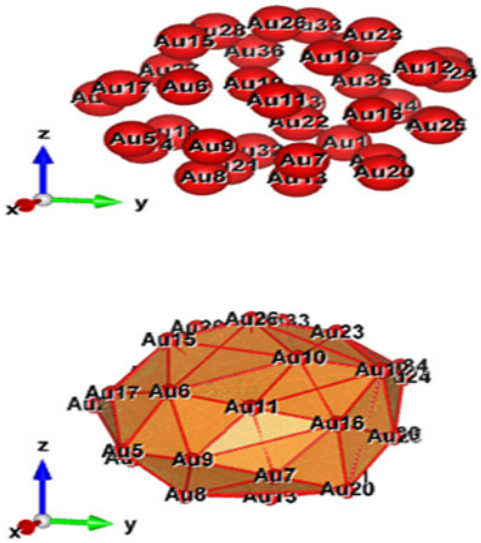

Figure 1) *Au_{36} (C_1); Style (Space-filling [up], Polyhedral [down]): The lowest energy geometrical structure of the Au_{36} cluster. Standard orientation of crystal shape at ΔE=0.*

Table 1
The normal modes (NVM) and the vibrational frequencies (ω_i) of Au_{36} at ΔE=0

NVM (3N-6)	$\omega_{i\,(cm^{-1})}$	NVM (3N-6)	$\omega_{i\,[cm-1]}$	NVM (3N-6)	$\omega_{i\,(cm^{-1})}$	NVM (3N-6)	$\omega_{i\,(cm^{-1})}$
1	4.38	30	44.97	59	108.3	88	212.4
2	5.97	31	46.02	60	112.58	89	214.94
3	7.62	32	47.1	61	116.64	90	221.29
4	8.34	33	47.67	62	119.95	91	221.84
5	10.02	34	49.62	63	121.54	92	226.14
6	10.38	35	51.6	64	125.09	93	232.36
7	12.94	36	52.79	65	130.95	94	235.23
8	13.11	37	54.81	66	135.05	95	239.78
9	14.39	38	57.29	67	137.05	96	245.21
10	15.62	39	58.96	68	141.51	97	249.46
11	17.16	40	59.72	69	143.49	98	255.07
12	17.85	41	64.46	70	147.07	99	266.58
13	19.29	42	65.25	71	151.47	100	269.13
14	20.49	43	67.39	72	155.24	101	279.52
15	21.76	44	68.25	73	159.17	102	302.78
16	23.96	45	70.27	74	165.82	103	-
17	25	46	74.38	75	168.54	104	-
18	25.64	47	76.33	76	169.41	105	-
19	27.39	48	78.39	77	177.04	106	-
20	28.49	49	79.86	78	177.85	107	-
21	29	50	81.29	79	181.16	108	-
22	30.13	51	82.99	80	182.49	109	-
23	32.57	52	86.57	81	186.85	110	-
24	33.18	53	88.4	82	194.38	111	-
25	34.85	54	92.48	83	196.94	112	-
26	35.92	55	95.09	84	198.1	113	-
27	37.48	56	98.51	85	200.71	114	-
28	39.36	57	101.53	86	203.73	115	-
29	43.59	58	103.79	87	209.54	116	-

The triple state degeneracy (ω_i)

We do not find anything; it is clearly revealed through our spectrum calculations that have not occurred.

The vibrational frequency (ω_i)

range of the cluster Au_{39} at $\Delta E=0$

Table 3 shows the low (at the least) and the high (at the most) frequency range of the cluster Au_{39}, which occurs between 0.98 and 304.48 cm^{-1}, and the lowest energy geometrical structural view can be seen in Figure 3. Firstly, the cluster has some low frequencies (ω_{min}) between 0.98 cm^{-1}-9.50 cm^{-1}, which is only for the very first 7 NVM, which comes even below the scale of Far Infrared FIR, IR-C 200 cm^{-1} to 10 cm^{-1}. Secondly, for the 8 NVM to 94 NVM, the frequency ranges are occurred between 10.38-198.61 cm^{-1}, which

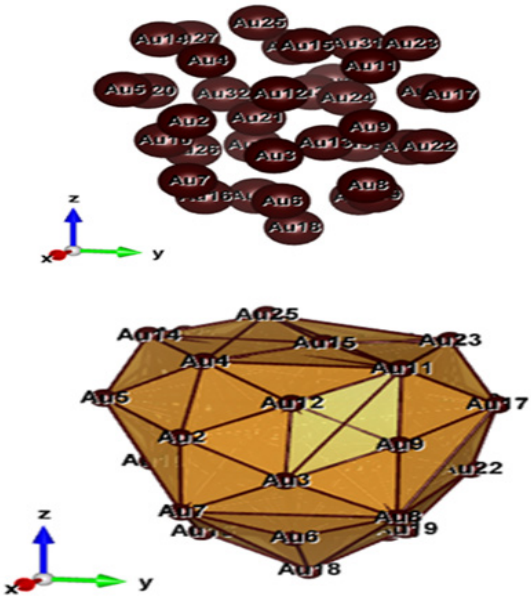

Figure 2) *Au_{37} (C_1); Style (Space-filling [left], Polyhedral [right]): The lowest energy geometrical structure of the Au_{37} cluster. Standard orientation of crystal shape at $\Delta E=0$.*

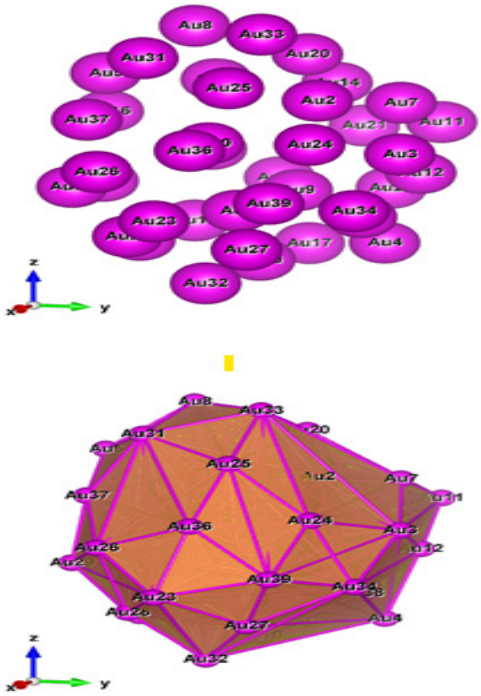

Figure 3) *Au_{39} (C_1); Style (Space-filling [left], Polyhedral [right]): The lowest energy geometrical structure of the Au_{39} cluster. Standard orientation of crystal shape at $\Delta E=0$*

TABLE 2
The Normal modes (NVM) and the vibrational frequencies (ω_i) of Au_{37} at $\Delta E=0$

NVM (3N-6)	ω_i (cm^{-1})	NVM (3N-6)	ω_i (cm^{-1})	NVM (3N-6)	ω_i (cm^{-1})	NVM (3N-6)	ω_i (cm^{-1})
1	4.7	30	40.44	59	95.98	88	201.54
2	5.57	31	41.58	60	100.6	89	203.22
3	6.12	32	43.18	61	103.21	90	206.19
4	6.48	33	43.59	62	106.95	91	210.95
5	7.25	34	44.78	63	107.99	92	214.22
6	9.59	35	46.75	64	111.04	93	216.98
7	10.44	36	48.3	65	115.47	94	219.55
8	10.62	37	49.48	66	118.7	95	223.47
9	11.72	38	51.14	67	120.12	96	228.96
10	13.03	39	52.11	68	123.96	97	236.19
11	14.85	40	54.23	69	127.65	98	244.5
12	16.74	41	56.77	70	130.9	99	257.14
13	17.18	42	57.68	71	139.09	100	264.55
14	17.87	43	59.16	72	142.88	101	267.19
15	19.16	44	62.37	73	146.46	102	274.03
16	22.28	45	63.86	74	154.56	103	286.27
17	23.29	46	66.45	75	156.19	104	294.69
18	24.98	47	69	76	159.96	105	300.67
19	26.61	48	70.08	77	163.89	106	-
20	28.5	49	72.15	78	165.34	107	-
21	29.07	50	74.4	79	167.89	108	-
22	29.95	51	78.31	80	172.55	109	-
23	31.5	52	80.63	81	175.83	110	-
24	32.12	53	82.92	82	185.66	111	-
25	33.75	54	83.89	83	186.42	112	-
26	35.74	55	86.4	84	187.35	113	-
27	36.46	56	87.69	85	189.15	114	-
28	37.3	57	91.87	86	196.88	115	-
29	39.96	58	95.22	87	197.79	116	-

TABLE 3
The Normal Modes (NVM) and the vibrational frequencies (ω_i) of Au_{39} at $\Delta E=0$

NVM (3N-6)	ω_i (cm^{-1})	NVM (3N-6)	ω_i (cm^{-1})	NVM (3N-6)	ω_i (cm^{-1})	NVM (3N-6)	ω_i (cm^{-1})
1	0.98	30	35.47	59	88.84	88	178.33
2	2.45	31	36.2	60	90.61	89	184.04
3	3.65	32	38.72	61	93.88	90	188.67
4	6.26	33	39.71	62	94.48	91	189.62
5	7.3	34	41.64	63	98.71	92	191.1
6	8.81	35	42.88	64	101.56	93	195.07
7	9.5	36	43.47	65	103.1	94	198.61
8	10.38	37	44.93	66	104.42	95	202.26
9	11.12	38	46.37	67	107.12	96	206.97
10	12.52	39	48.47	68	108.12	97	209.26
11	12.78	40	49.33	69	113.48	98	212.2
12	13.91	41	49.77	70	117.12	99	218.05
13	14.98	42	51.37	71	122.33	100	222.72
14	16.82	43	53.25	72	125.21	101	225.94
15	18.3	44	53.67	73	126.61	102	226.95
16	18.97	45	56.07	74	132.96	103	229.29
17	20.05	46	56.83	75	135.78	104	232.75
18	20.35	47	58.43	76	138.05	105	241.6
19	22.63	48	60.97	77	139.61	106	248.58
20	22.94	49	61.77	78	143.6	107	254.79
21	23.04	50	63.74	79	147.6	108	259.57
22	25.16	51	66.17	80	148.45	109	269.84
23	25.93	52	67.94	81	155.8	110	279.22
24	27.88	53	70.88	82	157.65	111	304.48
25	28.21	54	73.05	83	163.5	112	-
26	29.16	55	76.56	84	168.95	113	-
27	30.2	56	77.91	85	172.36	114	-
28	32.55	57	82.53	86	173.81	115	-
29	33.49	58	83.5	87	175.25	116	-

comes within the range of Far Infrared FIR, IR-C 200- 10 cm^{-1}. Thirdly, for the rest of the 95 NVM to 111 NVM, are having the maximum high frequencies, which are ((ω_i)-202.26 cm^{-1} to 304.48 cm^{-1}) falling within the range of Mid Infrared MIR, IR-C 3330 cm^{-1} to 200 cm^{-1}.

The double and the triple state degeneracy (ω_i)

[{12.52, 12.78}; {18.30, 18.97}; {20.05, 20.35}; {22.63, 22.94}; {25.16, 25.93}; {49.33, 49.77}; {53.25, 53.67} and {56.07 56.83}] in cm^{-1}.

The triple state degeneracy (ω_i)

We do not find anything; it is clearly revealed through our spectrum calculations that have not occurred.

The vibrational frequency (ω_i) range of the cluster Au_{40} at ΔE=0

Table 4 shows the low (at the least) and the high (at the most) frequency range of the cluster Au_{40}, which occurs between 2.55 cm^{-1} and 282.94 cm^{-1}, and the lowest energy geometrical structural view can be seen in Figure 4. Firstly, the cluster has some low frequencies (ω_{min}) between 2.55 cm^{-1} to 9.39 cm^{-1}, which is only for the very first 6 NVM, which comes even below the scale of Far Infrared FIR, IR-C 200 cm^{-1} to 10 cm^{-1}. Secondly, for the 7NVM to 95 NVM, the frequency ranges are occurred between 10.65 cm^{-1} to 195.06 cm^{-1}, which comes within the range of Far Infrared FIR, IR-C 200 cm^{-1} to 10 cm^{-1}. Thirdly, the rest of the 96 NVM to 114 NVM, are having the maximum high frequencies, which are ((ω_i)-202.65 cm^{-1} to 282.94 cm^{-1}) falling within the range of Mid Infrared MIR, IR-C 3330 cm^{-1} to 200 cm^{-1}.

The double state degeneracy (ω_i)

[{11.10, 11.98}; {13.19, 13.52}; {18.41, 18.60}; {20.17, 20.92}; {23.34, 23.66}; {31.03, 31.58}; {33.57, 33.68}; {38.89, 38.94}; {60.24, 60.67}; {64.16, 64.34}; {100.12, 100.89}; {165.21, 165.61} and {192.24, 192.68}] in cm^{-1}.

The triple state degeneracy (ω_i)

We do not find anything; it is clearly revealed through our spectrum calculations that have not occurred.

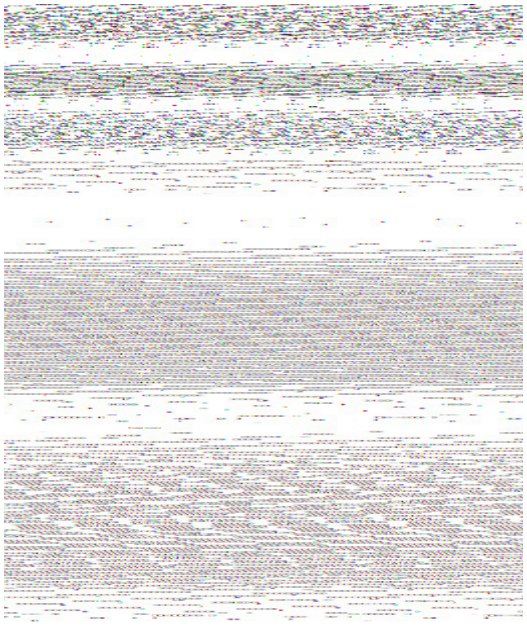

Figure 4) *Au_{40} (C_1); Style (Space-filling [left], Polyhedral [right]): The lowest energy geometrical structure of the Au_{40} cluster. Standard orientation of crystal shape at ΔE=0*

Size and the shape effects

In Table 5, the third column shows the spectral ranges that have been influenced with respect to the size of the clusters, the shape of the structures, and the arrangement of the atoms (inner core, and the overall outer surface of the edges), as well as the short and the long range interactions due to the inter-nuclear attraction and the repulsive energies.

CONCLUSION

We are first to present, the vibrational frequencies of bigger-sized clusters (Au_{36}, $Au_{37,}$ Au_{39} and Au_{40}) and the shell-like structure of the re-optimized structures, at ΔE=0, by using the numerical finite-differentiation method with the DFTB approach. We found the vibrational spectrum, the minimum starting, and the maximal end ranges that vary between 0.98 $cm^{-1}$and 304.48 cm^{-1} at ΔE=0. The occupancy of the multiple double and the triple state degeneracy is revealed on the gold atomic clusters, Au_{36}, Au_{37}, Au_{39} and Au_{40}. More the double-state degeneracy may depend on the nearest neighboring atoms, and their interactions, as well as the zig-zag circumstances of the outermost surface surrounded by them. We are able to see, a maximum, of 13 total pairs have occurred on the Au_{40} cluster, which is very special to the others.

Above all, we have pinpointed the correct location of the spectrum, through Far Infrared FIR, IR-C 200 cm^{-1} to 10 cm^{-1}, and Mid Infrared MIR, IR-C 3330 cm^{-1} to 200 cm^{-1}, and even outside of this range. In addition to that, our prediction will help the researchers to develop a range of potential

TABLE 4
The Normal modes (NVM) and the vibrational frequencies (ω_i) of Au_{40} at ΔE=0.

NVM (3N-6)	ω_i (cm^{-1})	NVM (3N-6)	ω_i (cm^{-1})	NVM (3N-6)	ω_i (cm^{-1})	NVM (3N-6)	ω_i (cm^{-1})
1	2.55	30	34.85	59	83.68	88	174.29
2	4.14	31	35.97	60	84.14	89	179.75
3	6.12	32	37.67	61	87.77	90	180.67
4	7.81	33	38.89	62	89.33	91	187.99
5	8.54	34	38.94	63	91.82	92	189.46
6	9.39	35	40.42	64	96.66	93	192.24
7	10.65	36	41.04	65	99.94	94	192.68
8	11.1	37	42.64	66	100.12	95	195.06
9	11.98	38	44.83	67	100.89	96	202.65
10	13.19	39	46.41	68	103.57	97	206.41
11	13.52	40	48.61	69	111.14	98	210.63
12	15.13	41	49.33	70	114.92	99	214.72
13	17.71	42	51.04	71	118.04	100	221.2
14	18.41	43	52.27	72	120.91	101	223.58
15	18.6	44	54.05	73	123.88	102	228.32
16	20.17	45	56.5	74	127.89	103	230.08
17	20.92	46	58.92	75	131.06	104	231.76
18	23.34	47	60.24	76	135.96	105	238.29
19	23.66	48	60.67	77	138.51	106	239.02
20	24.19	49	64.16	78	141.84	107	244.35
21	25.6	50	64.34	79	144.78	108	246.71
22	26.58	51	68.97	80	151.84	109	253.61
23	27.46	52	69.76	81	155.03	110	254.71
24	28.47	53	70.81	82	158.68	111	263.59
25	29.86	54	72.22	83	159.92	112	266.41
26	31.03	55	73.45	84	165.21	113	270.79
27	31.58	56	76.78	85	165.61	114	282.94
28	33.57	57	79.49	86	171.11	115	-
29	33.68	58	81.47	87	172.51	116	-

TABLE 5
The double and the triple state degree of degeneracy of the clusters, Au_{36}, Au_{37}, Au_{39} and Au_{40} at ΔE = 0. Unfortunately, we do not find anything; it is clearly revealed through our spectrum calculations the triple state degree of degeneracy that has not occurred.

Gold Nanoclusters (AuNCs)	Point Groups (PG) Symmetry	Spectral Range (min - to -max) ω_i [cm^{-1}]	Double (D) & Triple (T) State Degeneracy [DT]{pairs}	Total Number of Pairs	Total Random Number (RN) of Different States of Equal Energy RN=(D*pairs+T*pairs)	Predicted Spectral Range Only for D, T-Degeneracies A: Far Infrared FIR, IR - C 200 - 10 cm^{-1} B: Mid Infrared MIR, IR - C 4000 - 200 cm^{-1} X: Lesser than both, A and B
Au_{36}	C_1	4.38-302.78	$D^6 T^0$	6	12	A, B
Au_{37}	C_1	4.70-300.67	$D^6 T^0$	6	12	A, X
Au_{39}	C_1	0.98-304.48	$D^8 T^0$	8	16	A
Au_{40}	C_1	2.55-282.94	$D^{13} T^0$	13	26	A

applications such as catalysis, biomedicine, imaging, optics, and energy conversion.

REFERENCES

1. Wu L, Fang W, Chen X. The photoluminescence mechanism of ultra-small gold clusters. Phys Chem Chem Phys. 2016;18(26):17320-5.
2. Andres RP, Bein T, Dorogi M, et al. Coulomb staircase at room temperature in a self-assembled molecular nanostructure. science. 1996;272(5266):1323-5.
3. Griffith WP. The Chemistry of the Rarer Platinum Metals. Inter-Science: New York. 1967:2-4.
4. Hartley FR. The chemistry of platinum and palladium: with particular reference to complexes of the elements. Appl Sci Publ; 1973.
5. Huang X. Polymer Ligand Stabilized Fluorescent Platinum Nanoclusters: Synthesis, Characterization, and Their Applications. Osaka University. 2016.
6. Siegel RW. Nanostructured materials mind over matter. Nanostructured Materials. 1994;4:121-38
7. Huang X, Li Z, Yu Z, et al. Recent Advances in the Synthesis, Properties, and Biological Applications of Platinum Nanoclusters. J Nanomater. 2019:6248725.
8. Choi YC, Lee HM, Kim WY, et al. How can we make stable linear monoatomic chains? Gold-cesium binary subnanowires as an example of a charge-transfer-driven approach to alloying. Phys Rev lett. 2007;98(7):076101.
9. Li J, Liu Y, Zhang J, et al. Density functional theory study of the adsorption of hydrogen atoms on Cu2X (X=3d) clusters. Chem Phys Lett. 2016;651:137-43.
10. Chuanchuan Z, Haiming D, Xin L, et al. Staticand dynamical isomerization of Cu38 cluster. Scientific Reports 2019;9:7564.
11. Garzon IL, Posada-Amarillas A. Structural and vibrational analysis of amorphous Au 55 clusters. Physical Review B. 1996;15;54(16):11796.
12. Bravo-Pérez G, Garzón IL. Novaro O. Ab initio study of small gold clusters. J Mol Struct: THEOCHEM. 1999;15;493(1-3):225-31.
13. Bravo-Perez G, Garzon IL, Novaro O. Non-additive effects in small gold clusters. Chem Phys Lett. 1999;313:655-64.
14. Sauceda HE, Mongin D, Maioli P, et al. Vibrational properties of metal nanoparticles: Atomistic simulation and comparison with time-resolved investigation. J Phys Chem C. 2012;116:25147-56.
15. Sauceda HE, Pelayo JJ, Salazar F, et al. Vibrational spectrum, caloric curve, low-temperature heat capacity, and Debye temperature of sodium clusters: The Na139+case. J Phys Chem C. 2013;117:11393-8.
16. Sauceda HE, Salazar F, Perez LA, et al. Size and shape dependence of the vibrational spectrum and low-temperature specific heat of Au nanoparticles. J Phys Chem C. 2013;117:25160-8.
17. Sauceda HE, Garzon IL. Structural determination of metal nanoparticles from their vibrational (phonon) density of states. J Phys Chem C. 2015;119:10876.
18. Dugan N, Erkoc S. Stability analysis of graphene nanoribbons by molecular dynamics simulations. Physica status solidi (b). 2008;245(4):695-700.
19. Dong Y, Springborg M. Global structure optimization study on Au2-20. Eur Phys J D. 2007;43:15-18.
20. Warnke I. Heat Capacities of Metal Clusters. Diploma Thesis (Research Assistant and Diploma Research), Saarland University. 2007.
21. Dvornikov M. Formulae of numerical differentiation. 2004.
22. Porezag D, Frauenheim Th, Kohler Th, et al. Construction of tight-binding-like potentials on the basis of density-functional theory: Application to carbon. Phys Rev B. 1995;51:12947.
23. Seifert G, Schmidt R. Molecular dynamics and trajectory calculations: The application of an LCAO-LDA scheme for simulations of cluster-cluster col-lisions. New J Chem. 1992;16:1145.
24. Seifert G, Porezag D,. Frauenheim Th. Calculations of molecules, clusters, and solids with a simplified LCAO-DFT-LDA scheme. Int J Quantum Chem. 1996;58:185-9.
25. Seifert G. Tight-Binding Density Functional Theory: An Approximate Kohn-Sham DFT Scheme. J Phys Chem A. 2007;111:5609-5613.
26. Press WH, Teukolsky SA, Vetterling WT, et al. Numerical Recipes in Fortran.
27. Cambridge University Press. 2007 Vishwanathan K. Bonding Forces and Energies on the Potential Energy Surface (PES) of the Optimized Gold Atomic Clusters by a Differentiation Step-Size (ds = ± 0.01 a.u.) via DFTB Method. Nanosci Technol. 2018;5:1-4.